

Breakup threshold anomaly in the elastic scattering of ${}^6\text{Li}$ on ${}^{27}\text{Al}$

J. M. Figueira,^{1,2,*} J. O. Fernández Niello,¹ D. Abriola,¹ A. Arazi,¹ O. A. Capurro,¹ E. de Barbará,¹ G. V. Martí,¹ D. Martínez Heimann,¹ A. E. Negri,¹ A. J. Pacheco,¹ I. Padrón,^{3,†} P. R. S. Gomes,³ J. Lubian,³ T. Correa,³ and B. Paes³

¹Laboratorio TANDAR, Comisión Nacional de Energía Atómica, Av. General Paz 1499, 1650 San Martín, Buenos Aires, Argentina

²Departamento de Física, FCEyN, Universidad de Buenos Aires, Ciudad Universitaria, Pabellón 1, 1428 Buenos Aires, Argentina

³Instituto de Física, Universidade Federal Fluminense, Av. Litoranea s/n, Gragoatá, Niterói, R.J., 24210-340, Brazil

(Received 3 November 2006; published 17 January 2007)

Elastic scattering of the weakly bound ${}^6\text{Li}$ on ${}^{27}\text{Al}$ was measured at near-barrier energies. The data analysis was performed using a Woods-Saxon shape optical potential and also using the double-folding São Paulo potential. The results show the presence of the breakup threshold anomaly (BTA), an anomalous behavior when compared with the scattering of tightly bound nuclei. This behavior is attributed to a repulsive polarization potential produced by the coupling to the continuum breakup states.

DOI: [10.1103/PhysRevC.75.017602](https://doi.org/10.1103/PhysRevC.75.017602)

PACS number(s): 25.70.Bc, 24.10.Ht, 25.70.Mn

It is well accepted that in the elastic scattering of heavy ions at energies near the Coulomb barrier, the real and the imaginary parts of the optical potential show an energy dependence, known as threshold anomaly (TA) [1,2]. This behavior is characterized by a localized peak in the real part of the potential and by the decrease of the imaginary part of the potential as the bombarding energy decreases towards the Coulomb barrier. At higher energies, both the real and the imaginary potentials are energy independent.

The TA may be ascribed mainly to the coupling of the elastic scattering to other reaction channels that produces an attractive polarization potential ΔV , leading to a real potential $V_{\text{eff}} = V_0 + \Delta V$, where V_0 is the real potential at higher energies. This additional attraction due to the increase of the real potential decreases the Coulomb barrier and leads to the usual sub-barrier fusion enhancement that is observed in several systems. The dependence of the imaginary potential on the energy reflects the closure of nonelastic peripheral channels at energies near and below the Coulomb barrier. The correlation between the real and the imaginary potentials is due to the causality that imposes the condition that no scattered wave emerges before the incident wave reaches the target. The mathematical relation involving causality and the TA is the dispersion relation, which connects the real and imaginary potentials through a principal value integral [3,4].

This situation may change substantially for systems that involve weakly bound nuclei. In these cases there is a strong coupling of the elastic channel with the breakup process [5], which may have a much larger cross section than fusion at sub-barrier energies. The imaginary potential strength does not necessarily diminish when the bombarding energy decreases and the TA may no longer be present. Actually, it has been recently proposed [6] a new phenomenon for this kind of behavior, called breakup threshold anomaly (BTA). In those systems, the coupling to the breakup channel continues to be important even for energies below the barrier, thus the

threshold could occur at an energy below the barrier itself, and therefore the imaginary potential could even increase at lower energies. In that case, due to the dispersion relation the real part of the potential should decrease. This can be related to a repulsive polarization potential produced by the coupling to the continuum breakup states, leading to a hindrance of the sub-barrier fusion cross section. The BTA phenomenon has been clearly observed in the scattering of ${}^6\text{Li}+{}^{208}\text{Pb}$ system [6]. On the other hand, in the ${}^6\text{Li}+{}^{138}\text{Ba}$ [7,8] and ${}^9\text{Be}+{}^{64}\text{Zn}$ [8–10] systems, it was possible to experimentally observe the increase of the imaginary potential for only one energy value and, consequently, the BTA could not be unequivocally identified.

In this work we describe the measurement of elastic scattering angular distributions in the ${}^6\text{Li}+{}^{27}\text{Al}$ system from energies below the Coulomb barrier (about 8.0 MeV) up to more than twice this value. The ${}^6\text{Li}$ nuclide is the most loosely bound stable nucleus, therefore the breakup process is expected to be important (for this projectile, the alpha-deuterium breakup threshold energy is 1.48 MeV). Thus, the study of the elastic scattering in the ${}^6\text{Li}+{}^{27}\text{Al}$ system contributes to the understanding of the role of the breakup process on the elastic scattering of light systems. In order to have results which are independent of the data analysis, two different potentials were used. The results are compared with those of recent measurements of the elastic scattering of ${}^7\text{Li}$ on ${}^{27}\text{Al}$ [11].

Beams of ${}^6\text{Li}$ at energies of 7, 8, 10, 12, and 18 MeV were delivered by the 20 UD tandem accelerator at the TANDAR Laboratory in Buenos Aires irradiating $75 \mu\text{g}/\text{cm}^2$ thick ${}^{27}\text{Al}$ foils. Typical beam currents were of the order of 10 nA. An array of eight silicon surface barrier detectors placed inside a 30-in.-diameter scattering chamber was used to measure elastic-scattering angular distributions, which were taken in steps of 2° or 5° , depending on the bombarding energy and angular range. The angular resolution of all the detectors was better than 0.5° and their energy resolution ranged from 0.5% to 1.3%. Figure 1 shows a typical energy spectrum, where one can see that the elastic peak is well separated from the scattering on ${}^{12}\text{C}$ and ${}^{16}\text{O}$ target contaminants. Elastic-scattering cross sections were obtained from the number of counts in these peaks at each energy,

*Electronic address: figueira@tandar.cnea.gov.ar

†Permanent address: CEADEN, P.O. Box 6122, Havana, Cuba.

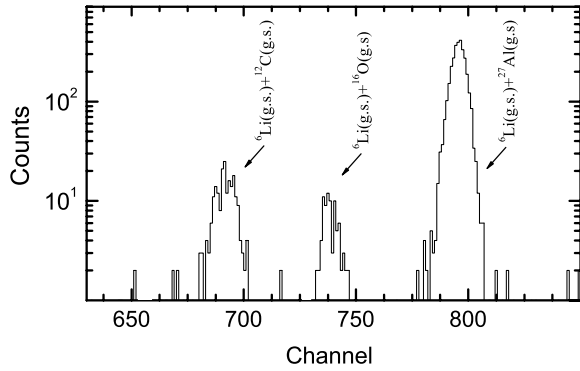


FIG. 1. Energy spectrum for the ${}^6\text{Li}+{}^{27}\text{Al}$ system taken at $E_{\text{Lab}} = 7$ MeV and $\theta_{\text{Lab}} = 40.0^\circ$. Exit channels are indicated in the figure.

normalized by the integrated current obtained with the aid of an electron-suppressed Faraday cup and a monitor detector placed at 15° . The estimated overall uncertainty of the cross sections ranges from 5% to 15%. Figure 2 shows the angular distributions of the elastic-scattering cross sections divided by the corresponding Rutherford cross sections. The curves are the best fits obtained, as it will be described in the following.

For the data analysis we used two different potential models, (i) a phenomenological Woods-Saxon potential (WSP), and (ii) the São Paulo folding potential (SPP) [12,13]. The ECIS code [14] was used for both models.

The phenomenological potential used in the calculations was energy dependent but with fixed geometric parameters (reduced radius and diffuseness). The real part was a Woods-Saxon characterized by a depth V , a reduced radius r_0 and a diffuseness a . The imaginary part consists of two terms, a volume Woods-Saxon term and a surface term, described by W , r_{i0} , a_i and WS , r_{si0} , a_{si} , respectively. The volume term takes the fusion channel into account, whereas the surface term, which is proportional to the derivative of a Woods-Saxon shape, accounts for the flux of the quasi-elastic channels.

In order to obtain the starting parameters, we performed a global best fit procedure for all energies. Then, we fixed the volume imaginary potential as $W = 50$ MeV, $r_{i0} = 1.09$ fm, and $a_i = 0.22$ fm. The reduced radii of the real and the surface imaginary potentials were also fixed at $r_0 = 1.30$ fm and

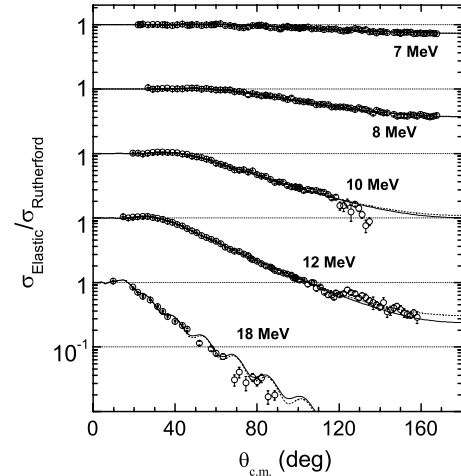


FIG. 2. Elastic scattering data for the system ${}^6\text{Li}+{}^{27}\text{Al}$. The solid lines represent the best fits using the Woods-Saxon potential and the dotted lines correspond to São Paulo folding potential fits.

$r_{si0} = 1.30$ fm, while the diffuseness took the values $a = 0.53$ fm and $a_{si} = 0.711$ fm, respectively. The adjustable parameters were the depths of these potentials. They were derived from the best fit procedure for each angular distribution.

The comparison of the potentials at different energies was performed at the sensitivity radius R_s , i.e., the approximate radius at which all the potentials that fit the data intersect [15]. The sensitivity radius for the real as well as for the imaginary parts, R_{SV} and R_{SW} , respectively, were evaluated at each energy by selecting a set of slightly modified diffuseness parameters a (taken in steps of 0.025 fm around the best value) and adjusting both the radius parameter and the potential depth to fit the data. In this way, different families of optical model potentials with similar values of χ^2/point were obtained. The derived sensitivity radii at different energies are not strictly constant, but they fluctuate around average values of $R_{SV} = 8.7 \pm 0.3$ fm and $R_{SW} = 9.6 \pm 0.3$ fm.

Table I shows, for each energy, the derived parameters for the Woods-Saxon potential taken at an average sensitivity radius $\bar{R}_s = 9.2$ fm. These derived values are shown in Fig. 3. The solid line corresponding to WS is an adjustment based on the functional schematic dependence of the surface imaginary

TABLE I. Energy dependence of the ${}^6\text{Li}+{}^{27}\text{Al}$ optical model parameters (values of V and WS evaluated at an average sensitivity radius $\bar{R}_s = 9.2$ fm) using the phenomenological potential with fixed geometry and the normalization factors (N_R and N_I) of the folding São Paulo potential. For the phenomenological potential the reduced radii and diffuseness of the real and surface imaginary parts were $r_0 = r_{si0} = 1.30$ fm and $a = 0.53$ fm and $a_{si} = 0.711$ fm, respectively, and the parameters for the volume imaginary part were $W = 50$ MeV, $r_{i0} = 1.09$ fm and $a_i = 0.227$ fm. The fourth and the seventh columns show the χ^2/point values obtained using the Woods-Saxon and the São Paulo potentials, respectively.

$E_{\text{c.m.}}$ (MeV)	V (MeV)	WS (MeV)	χ^2/point	N_R	N_I	χ^2/point
5.7	0.046 ± 0.007	0.30 ± 0.01	1.14	0.83 ± 0.08	2.6 ± 0.3	1.15
6.5	0.194 ± 0.005	0.15 ± 0.02	1.47	1.66 ± 0.04	2.0 ± 0.2	1.44
8.2	0.144 ± 0.001	0.110 ± 0.007	3.68	1.20 ± 0.03	1.3 ± 0.1	3.85
9.8	0.149 ± 0.001	0.126 ± 0.004	3.17	1.28 ± 0.01	1.35 ± 0.03	2.97
14.7	0.356 ± 0.007	0.09 ± 0.02	16.2	2.5 ± 0.2	2.4 ± 0.3	18.2

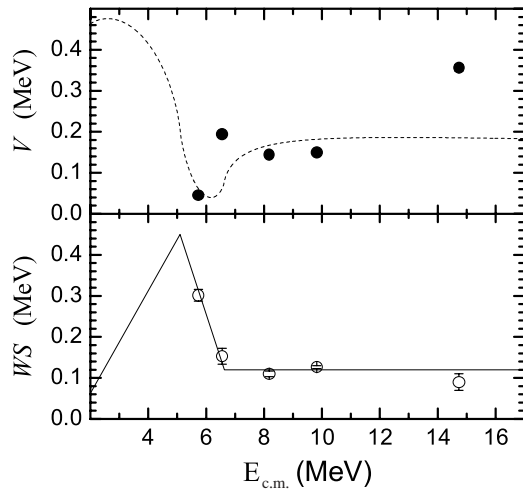


FIG. 3. Values of the real and imaginary parts of the optical potential at the average sensitivity radius $\bar{R}_s = 9.2$ fm, for the system ${}^6\text{Li}+{}^{27}\text{Al}$. See text for more details.

potential given in [6]. From this, the real part V , represented by the dashed line, is obtained using the dispersion relation. One can observe that, at low energies, the imaginary potential increases whereas the real potential drops leading to the breakup threshold anomaly.

As a second approach to the data analysis we used the São Paulo potential [12,13]. This double-folding potential was derived in the framework of an extensive systematization of nuclear densities. The energy dependence of the bare potential was accounted for by a model based on the Pauli nonlocal nature of the interaction of exchange of nucleons between projectile and target. This potential is able to describe a large variety of systems in a very wide energy range [16] and different reaction channels [17]. In the SPP, the imaginary part of the interaction is assumed to have the same shape of the real part, with just one single adjustable parameter related to its strength. Details concerning the SPP have been described in many papers and can be obtained, for instance, in Refs. [11–13,16,17]. In the fit procedure, the adjustable parameters were the normalization factors of the real and imaginary parts of the potential (N_R and N_I , respectively). The results of the fits are shown as dashed curves in Fig. 2. The energy dependence of the real and imaginary parts of the SPP are shown in Fig. 4. The dashed line for N_R is obtained by means of the dispersion relation using the same procedure as in the case of the phenomenological potential previously described. One can observe a very similar result, as compared

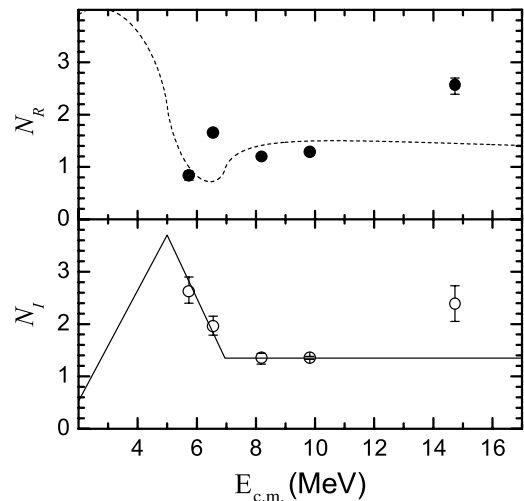


FIG. 4. Normalization factors of the real and imaginary potential (N_R and N_I) for ${}^6\text{Li}+{}^{27}\text{Al}$, as a function of the energy. See text for more details.

to the WSP approach. The presence of the breakup threshold anomaly is clearly noticed.

In conclusion, we can observe a rather different behavior in the elastic scattering of ${}^6\text{Li}$ (present work) and ${}^7\text{Li}$ [11] on ${}^{27}\text{Al}$. For both projectiles the usual threshold anomaly is not present, which can be attributed to the repulsive polarization potential produced by the coupling to the continuum breakup states. However, there are, indeed, important differences between the two Li isotopes: On the one side, ${}^6\text{Li}$ has a much lower threshold energy for alpha breakup than ${}^7\text{Li}$ (almost 1 MeV lower); on the other side, ${}^7\text{Li}$ has one bound excited state at 0.48 MeV, whereas ${}^6\text{Li}$ has none. Therefore, the couplings to breakup channels should be much stronger in the ${}^6\text{Li}$ scattering than in the ${}^7\text{Li}$ case, and consequently the repulsive polarization potential is much stronger on the ${}^6\text{Li}$ scattering than on the ${}^7\text{Li}$. So, the strength of this coupling on the ${}^7\text{Li}$ scattering is enough to destroy the usual threshold anomaly and leaves the real and imaginary parts of the potential as energy independent, compensating the attractive polarization potential due to inelastic and transfer channels. In the ${}^6\text{Li}$ case the repulsive polarization potential predominates, thus leading to the so-called breakup threshold anomaly phenomenon.

Some of us (I.P., P.R.S.G., and J.L.) acknowledge the financial support of the CNPq (Brazil) and CLAF (I.P.). A.A., J.O.F.N., and A.J.P. are also members of the Consejo Nacional de Investigaciones Científicas y Técnicas, Argentina.

- [1] G. R. Satchler, Phys. Rep. **199**, 147 (1991).
- [2] M. A. Nagarajan, C. C. Mahaux, and G. R. Satchler, Phys. Rev. Lett. **54**, 1136 (1985).
- [3] C. Mahaux, H. Ngô, and G. R. Satchler, Nucl. Phys. **A449**, 354 (1986).
- [4] G. R. Satchler and W. Love, Phys. Rep. **55**, 183 (1979).

- [5] L. F. Canto, P. R. S. Gomes, R. Donangelo, and M. S. Hussein, Phys. Rep. **424**, 1 (2006).
- [6] M. S. Hussein, P. R. S. Gomes, J. Lubian, and L. C. Chamon, Phys. Rev. C **73**, 044610 (2006).
- [7] A. M. M. Maciel *et al.*, Phys. Rev. C **59**, 2103 (1999).
- [8] P. R. S. Gomes *et al.*, J. Phys. G **31**, S1669 (2005).
- [9] S. B. Moraes *et al.*, Phys. Rev. C **61**, 064608 (2000).

- [10] P. R. S. Gomes *et al.*, Phys. Rev. C **71**, 034608 (2005).
- [11] J. M. Figueira *et al.*, Phys. Rev. C **73**, 054603 (2006).
- [12] L. C. Chamon *et al.*, Phys. Rev. C **66**, 014610 (2002).
- [13] M. A. G. Alvarez *et al.*, Nucl. Phys. **A723**, 93 (2003).
- [14] J. Raynal, Phys. Rev. C **23**, 2571 (1981).
- [15] D. Abriola *et al.*, Phys. Rev. C **39**, 546 (1989).
- [16] L. R. Gasques, L. C. Chamon, P. R. S. Gomes, J. Lubian, Nucl. Phys. **A764**, 135 (2006).
- [17] J. J. S. Alves *et al.*, Nucl. Phys. **A748**, 59 (2005).